Rescaled Monte Carlo approach for magnetic systems: *Ab initio* thermodynamics of bcc iron

F. Körmann,* A. Dick, T. Hickel, and J. Neugebauer
Max-Planck-Institut für Eisenforschung GmbH, D-40237 Düsseldorf, Germany
(Received 10 February 2010; revised manuscript received 12 March 2010; published 19 April 2010)

A combined *ab initio* approach to calculate the thermodynamic properties of bcc iron including vibrational, electronic, and magnetic free-energy contributions is derived. Special emphasis is placed on the magnetic contribution that is obtained using the frozen-magnon approach combined with Monte Carlo (MC) calculations. The importance of spin quantum-mechanical effects has been studied for magnetically nonfrustrated model systems by comparing classical and quantum MC. Based on this analysis, we propose a rescaling scheme which allows an approximate *ad hoc* inclusion of the quantum effects into the classical MC simulations. The rescaled MC scheme is found to be robust with respect to the specific magnetic configuration and the lattice type and is therefore expected to yield an approximate yet reliable description of the magnetic contribution for cases where quantum MC calculations are not practical. Applying the method to bcc iron and combining the magnetic, vibronic and electronic contributions, we find an excellent agreement with experimental data for the heat capacity and free energy, both, below and above the Curie temperature.

DOI: 10.1103/PhysRevB.81.134425 PACS number(s): 71.15.−m, 75.40.Cx, 75.50.Bb

I. INTRODUCTION

A key prerequisite for the rapidly emerging field of quantum-mechanically guided materials design is the availability of efficient and accurate simulation techniques, which allow a reliable prediction of thermodynamic materials properties. A promising route toward this aim is the combination of density-functional theory (DFT) with concepts of statistical physics which was, e.g., shown to yield accurate predictions for a wide range of nonmagnetic materials.[1–3] However, the incorporation of magnetic excitations into those concepts, being of utmost importance for the description of many technologically important structural materials, such as, e.g., steels,[4–9] remains challenging.

An often employed approach to capture the magnetic free-energy contribution of systems with localized magnetic moments[7,9–16] is the mapping of DFT calculations onto an effective Heisenberg Hamiltonian,

$$\mathcal{H} = -\sum_{ij} J_{ij}\mathbf{S}_i\mathbf{S}_j \tag{1}$$

with *ab initio* derived exchange coefficients J_{ij}, which mediate the magnetic exchange between spins $\mathbf{S}_i$ localized at lattice sites i and j. Within a classical interpretation of this model, the $\mathbf{S}_i$ are given by continuous three-dimensional (3D) vectors whereas in the quantum case, they are represented by operators obeying the commutator rules for orbital moments and having discretized eigenvalues.

For most realistic systems, an exact analytical solution of Eq. (1) is not known. For the classical interpretation of Eq. (1), efficient classical Monte Carlo (cMC) techniques can, however, be used to provide the numerically exact solution for an arbitrary set of J parameters. In contrast to this, the quantum-mechanical extension of these techniques, the quantum Monte Carlo (QMC) approach,[17,18] has a limited applicability due to the so-called (negative) sign problem.[19,20] As a consequence, for realistic systems such as bcc iron, which are characterized by long-ranged positive as well as negative exchange integrals,[15] a QMC solution of Eq. (1) is generally not feasible. Therefore, Eq. (1) is usually either solved numerically using classical cMC calculations[10–13] or treated analytically via approximate approaches such as the random-phase approximation (RPA).[7,13–16]

In the present work, we propose an alternative scheme to calculate the thermodynamic properties of magnetic Heisenberg systems where magnetic frustrations are weak or absent. The approach is based on the numerically exact cMC of the classical Heisenberg model. The quantum-mechanical effects which are neglected in the classical treatment of Eq. (1) are afterward approximately included. The procedure is divided into two steps: first, we ensure the quantum-mechanically correct high-temperature limit of the free energy by aligning the calculated classical entropy to the analytically known quantum solution. Second, the impact of the neglected low-temperature quantum effects is estimated in Sec. II by a careful comparison of model systems for which the numerically exact quantum solution via QMC calculations is accessible. The comparison allows to formulate a semiempirical rescaling approach [in the following denoted as rescaled Monte Carlo (rMC)] which modifies the classical solution toward the quantum-mechanical counterpart and thus improves the classical description at lower temperatures. A central aim of this paper is to combine the rMC approach with *ab initio* computed exchange coefficients as well as *ab initio* vibronic and electronic free-energy contributions in order to achieve a reliable thermodynamic description of bcc iron over a large temperature range as an example of a realistic material system.

II. RESCALING CLASSICAL MONTE CARLO APPROACH

The use of DFT-based input parameters in Eq. (1) and the subsequent solution of the model by means of classical cMC is nowadays a standard and successful approach.[10–13] Nevertheless, having in mind that quantum effects are not accounted for within the cMC approach, a number of crucial questions arises: (i) how significant are quantum effects for

thermodynamic properties such as the heat capacity $C_V(T)$, the internal energy $U(T)$ or the magnetic free energy $F(T)$? (ii) Above which temperatures T and for which spin numbers S are classical calculations sufficient? (iii) Is there a practical scheme to estimate the magnitude and influence of quantum effects *without* having the quantum solution available, i.e., based solely on the classical results?

In order to tackle these questions, we have evaluated the thermodynamic properties for a set of carefully selected magnetic systems using the exact QMC data as a reference and comparing them with the corresponding data obtained employing the cMC approach. This comparison provides direct insight into the importance of quantum effects as a function of spin quantum number and temperature. The choice of the systems was limited to unfrustrated systems to avoid the negative sign problem in the QMC approach. We included a wide range of magnetic interactions (ferromagnetic/antiferromagnetic) for various 3D bulk lattice types (sc, bcc, and fcc) and used different numbers of interaction shells (one and two shells).

To allow for a convenient comparison of the results for various spin S, and in particular, for the classical limit $S\rightarrow\infty$, we introduce effective exchange parameters $\tilde{J}=S(S+1)J^{\mathrm{QM}}=S^2J^{\mathrm{CL}}$, where J^{QM} and J^{CL} are the nearest-neighbor exchange integrals, respectively, in the quantum and classical case. In the following, we express all energies in units of $\tilde{J}$ and temperatures in units of $\tilde{J}/k_B$.

All cMC and QMC calculations were performed using the ALPS code.[21] For both calculations, cMC and QMC (the Loop algorithm[18] in the stochastic series-expansion method is used), cluster updates were employed to calculate at least 2×10^5 steps for equilibrating the system and 2×10^6 steps for thermal averaging. All supercells contained 512 atoms. For each configuration, $\approx$400 temperatures were evaluated. These settings ensure statistical errors of less than $0.01k_B$ on C_V in the considered temperature range except for the region close to the critical temperature. Increasing the supercell to 1728 atoms results in a more pronounced peak in C_V at the critical temperature but has only a marginal effect on the formalism discussed below. In the following, we illustrate our findings on the example of a bcc lattice with ferromagnetic nearest-neighbor coupling. The other investigated systems yield very similar dependencies and conclusions and will be discussed in a compact way later.

Within the ALPS code, the specific-heat capacity C_V (shown in Fig. 1) for cMC and QMC is calculated by virtue of the fluctuation-dissipation theorem (see, e.g., Ref. 22). The critical temperature T_C was determined by the position of the peak in C_V. For all considered spin quantum numbers $(S=1/2,1,3/2,7/2)$, the classical and quantum solutions for C_V agree well for sufficiently high temperatures ($T\gtrsim3\tilde{J}/k_B$) while the quantum solution of $T_C(S)$ is rapidly approaching the classical one (indicated by a dashed line in Fig. 1) with increasing spin $T_C(S\rightarrow\infty)=T_C^{\mathrm{cMC}}\approx2$. For a detailed discussion of the dependence of $T_C(S)$, we refer to Ref. 23. The fact that the classical solution for the heat capacity does not vanish for $T\rightarrow0$ (giving rise to a diverging magnetic entropy), is a direct consequence of the classically nondiscretized excitation spectrum.

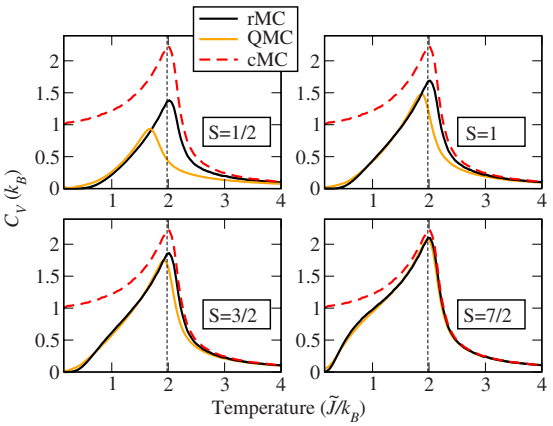

FIG. 1. (Color online) Heat capacity vs temperature for a $8\times8\times8$ bcc lattice with ferromagnetic nearest-neighbor coupling solved using cMC and QMC for $S=1/2,1,3/2,7/2$. For comparison, the rescaled cMC is shown.

From the numerical calculations, we further obtain the internal energy shown in Fig. 2. The cMC and QMC results agree for temperatures larger than $T\gtrsim3\tilde{J}/k_B$. For lower temperatures ($T\lesssim2\tilde{J}/k_B$), the difference between the classical and quantum solutions for the internal energy increase with decreasing spin quantum numbers. The largest difference occurs at $T=0$ and is equal to

$$U_{T=0}^{\mathrm{QM}}(S)-U_{T=0}^{\mathrm{CL}}=-[\tilde{J}_0S/(S+1)-\tilde{J}_0] \tag{2}$$

$$=\tilde{J}_0/(S+1) \tag{3}$$

with $\tilde{J}_0=\Sigma_{i,j}\tilde{J}_{ij}$.

The magnetic entropy S_{m} can be directly calculated from the heat capacity via integration either starting from low temperatures ($T=0$), or, if the maximum entropy $S_{\mathrm{m}}^{\mathrm{max}}=S_{\mathrm{m}}(T\rightarrow\infty)$ is known, from the high-temperature limit,

$$S_{\mathrm{m}}(T)=\int_0^T C_V(T')/T'\,dT' \tag{4}$$

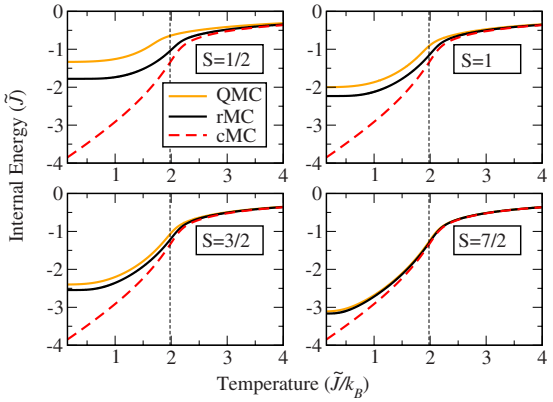

FIG. 2. (Color online) Internal energy vs temperature for a $8\times8\times8$ bcc lattice with ferromagnetic nearest-neighbor coupling solved using cMC and QMC for $S=1/2,1,3/2,7/2$. For comparison, the rescaled cMC is shown.

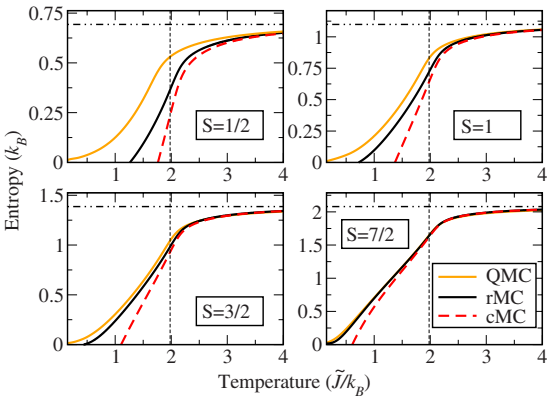

FIG. 3. (Color online) Magnetic entropy vs temperature for a $8\times8\times8$ bcc lattice with ferromagnetic nearest-neighbor coupling solved using cMC and QMC for $S=1/2,1,3/2,7/2$. For comparison, the rescaled cMC is shown.

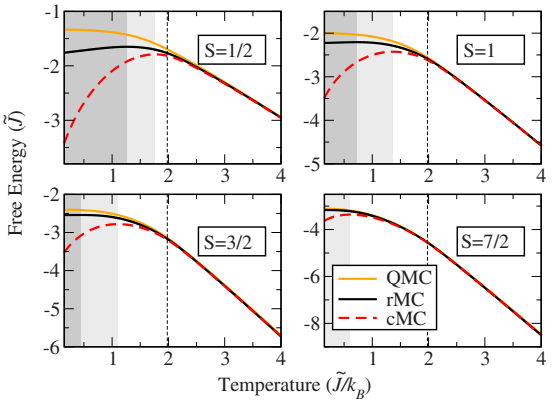

FIG. 4. (Color online) Free energy vs temperature for a $8\times8\times8$ bcc lattice with ferromagnetic nearest-neighbor coupling solved using cMC and QMC for $S=1/2,1,3/2,7/2$. For comparison, the rescaled cMC is shown. The range where the magnetic entropy of the aligned cMC and the rMC data becomes negative is highlighted by dark- and light-gray shading, respectively.

$$= S_{\mathrm{m}}^{\max} - \int_{T}^{\infty} C_V(T')/T'\,dT'. \tag{5}$$

For the quantum spin system represented by Eq. (1), the maximum entropy is spin dependent, $S_{\mathrm{m}}^{\max}(S)=\ln(2S+1)$, reflecting that in the high-temperature limit, all $2S+1$ spin states are equally occupied.

Due to the above-mentioned nonvanishing classical heat capacity at $T=0$, the corresponding magnetic entropy is not well defined for $T\to0$. To avoid the singularity, and to compare the classical results with the quantum results, we therefore align the classical maximum entropy to the quantum one using Eq. (5). The corresponding calculated entropies are shown in Fig. 3. With decreasing temperature, the entropy decreases from the paramagnetic limit given by $S_{\mathrm{m}}^{\max}(S)$ for fully disordered spins. Due to the treatment of spins as continues vectors, the classical solution overestimates the change in the magnetic entropy with temperature and yields a negative entropy at temperatures below a spin-dependent offset value $T^{\mathrm{off}}(S)$. The range of temperatures where cMC predicts a qualitatively wrong physical behavior of the system is shaded in Fig. 4 with light-gray color. Nevertheless, the alignment of the classical entropy to the quantum limit ensures that the free energy obtained with cMC for high temperatures ($T>2\tilde{J}/k_B$) accurately reproduces the quantum solution.

Despite the aligning scheme, the cMC approach still suffers from the neglect of the quantum effects, which turn out to significantly influence the free-energy data even at moderate temperatures (up to T_C). Having the importance of the classical approach for realistic materials science problems in mind, one of the central points of the present study is, therefore, the improvement of the cMC scheme in this temperature regime.

In the following, we develop a mean-field (MF)-based semiempirical approach which provides on the one hand a *practical* and efficient way to account for quantum effects and on the other hand, keeps the full flexibility of the cMC scheme. We concentrate on C_V since all other thermodynamic quantities can be easily calculated once the heat capacity is known.[24] The two main deviations between the classical and quantum solution are (a) the shape of C_V and (b) the spin dependence of the critical temperature. Since the latter would increase the complexity of our approach, we introduce a normalized temperature $t=T/T_C$ and focus on the deviations regarding the shape as a function of temperature and spin quantum number. These can be expressed in a compact form by introducing

$$f(t,S,\sigma) := C_V^{\mathrm{QMC}}(t,S,\sigma)/C_V^{\mathrm{cMC}}(t,\sigma), \tag{6}$$

where σ includes other dependencies apart from S and t, such as the lattice and/or magnetic configuration (e.g., number of interaction shells). In principle, if f is known, C_V^{QMC} can be computed solely based on the classical C_V^{cMC} solution. A numerical estimate of f can be obtained for the model systems such as those considered in Fig. 1 but is not available for configurations present in realistic material systems such as, e.g., bcc iron.

To analyze the shape and functional dependence of the scaling function f, we compute the ratio between the quantum-mechanical and the classical heat capacity for an extensive set of model systems where the QMC results are available. The set of chosen configurations σ includes different lattice structures (sc, bcc, and fcc) with nearest-neighbor ferromagnetic configurations ($J_1>0$) as well as antiferromagnetic configurations ($J_1<0$) for bcc and sc.[25] To check the robustness, we additionally included ferromagnetic configurations with second-nearest-neighbor interaction taking $J_2=2.5J_1>0$ and $J_2=5J_1>0$. The numerical results of Eq. (6) for two different spins, $S=1$ and $S=7/2$, are shown in Fig. 5. They show a strong scatter for high temperatures, where the quantum and classical solution should coincide, $f(t\gg1)\to1$. This is due to $C_V(t\gg1)\to0$ [see Eq. (6)] and the connected increase in the statistical errors. For the more important regime below $t=1$, however, the influence of σ on the function f is surprisingly weak and significantly smaller as compared to that of S and t.

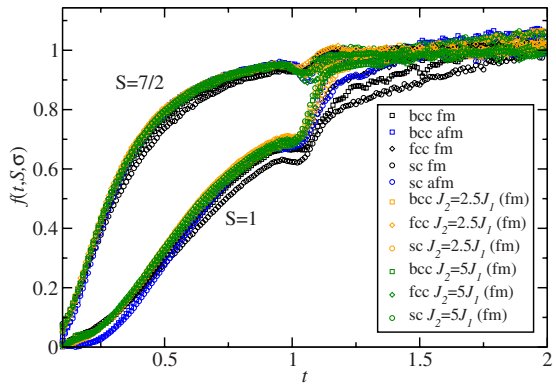

FIG. 5. (Color online) Numerically evaluated $f(t,S,\sigma)$ ratio (symbols) [see Eq. (6)] vs temperature for two spins $S=1$ and $S=7/2$ and various σ (lattice/magnetic configurations).

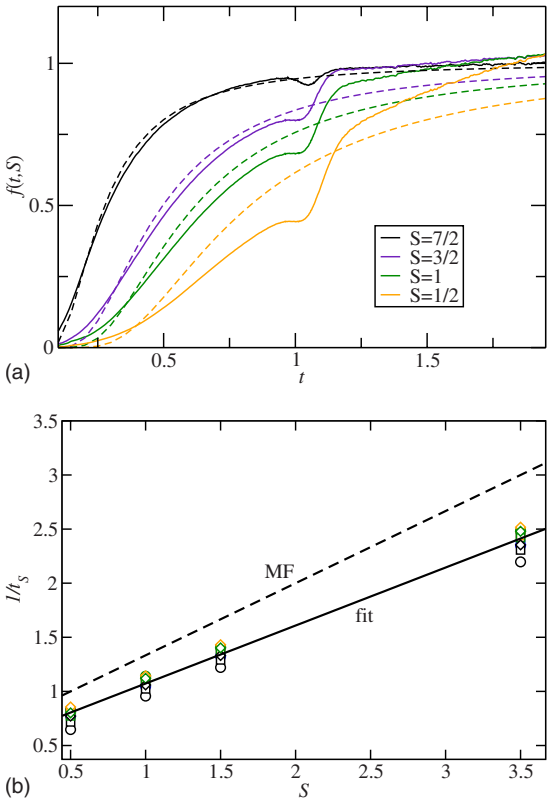

FIG. 6. (Color online) (a) Averaged data from Eq. (6) for different spin quantum numbers S of a bcc nearest-neighbor ferromagnet calculated using ≈400 temperature steps and corresponding fit $f^{\text{approx}}(t,S)$ obtained using Eq. (9) (dashed lines). (b) Linear relation of $1/t_S$ versus spin S. Symbols are defined as in Fig. 5

The observed weak dependence of the function f on the specific configuration σ that includes besides the crystal structure and magnetic state, also the range of interaction, is a central insight of this study and allows to neglect the σ dependence in first order. For a practical realization of this scheme, we determine the averaged scaling function $\bar{f}(t,S)$ that averages over all considered configurations. This function is expected to provide a good approximation also for realistic material systems, which have not been included in the current set of structures (due to the not accessible QM solution). A practical example will be given in Sec. III for the material system bcc iron. For an easy implementation of this approach, an analytical expression for $\bar{f}(t,S)$ is desirable. In the following, we discuss an empirical ansatz for this function, and test its accuracy/limits by comparing the rescaled cMC data based on the empirical ansatz with numerically exact results.

We start this discussion by considering the mean-field approximation of the Heisenberg model, which is known to describe thermodynamic properties at low temperatures reasonably well. An advantage of this approximation is the availability of analytical expressions for the magnetization in the quantum (Brillouin function) and in the classical (Langevin function) case. The resulting ratio of heat capacities, $f^{\text{MF}}(t,S)$, can therefore straightforwardly be computed. The shape of $f^{\text{MF}}(t)$ is in good agreement with that of f in the low-temperature regime except of a scaling factor due to the well-known overestimation of T_C in the MF approximation. To elaborate this in more detail, we analytically expand the low-temperature MF ratio (see Appendix) and obtain

$$f^{\text{MF}}(t \ll 1,S) \approx \left(\frac{2t_S/t}{\exp(t_S/t)}\right)^2 \tag{7}$$

with the spin-dependent temperature,

$$1/t_S = \alpha(S+1). \tag{8}$$

α is a proportionality factor. Its MF value is $\alpha^{\text{MF}} \equiv 2/3$.

For temperatures above the critical temperature ($t>1$), MF predicts $C_V \equiv 0$ due to the neglect of short-range order. Therefore, the analytic function Eq. (7) needs to be extended by an additional term, such that the resulting empirical function f^{approx} fulfills the following boundary conditions: First, for high temperatures, both solutions (quantum and classical) should coincide, i.e., $f^{\text{approx}}(t\to\infty,S)\to 1$. Second, the same should hold for an infinite spin quantum number, i.e., $f^{\text{approx}}(t,S\to\infty)\to 1$, reflecting that the classical model converges to the QM model in the limit of an infinite spin S. The choice

$$f^{\text{approx}}(t,S) := \left(\frac{2t_S/t}{\exp(t_S/t)-\exp(-t_S/t)}\right)^2 \tag{9}$$

obeys both conditions and provides a good fit of the data as will be discussed next.

In a second step, we fit the numerical exact scaling data Eq. (6) to the functional dependence of Eq. (9), using t_S as fit parameter. This procedure has first been performed for each of the investigated spin quantum numbers S, each structure (sc, bcc, and fcc) and magnetic configuration ($J>0$, $J<0$, $J_2=2.5J_1>0$, and $J_2=5J_1>0$) individually. As can be seen from Fig. 6(b), the used fitting function again appears to be remarkably independent of the configuration σ. Regarding the dependence on S, the parameter $1/t_S$ turns out to be nearly linearly proportional to the spin quantum number, similarly to MF in Eq. (8). This is consistent with the observation that the characteristic temperature above which the cMC and the QMC solution agree is inverse proportional to

TABLE I. Mean value of the mean deviation of the rescaled cMC with respect to the QMC calculations for the heat capacity, internal energy, entropy, and free energy in percent using $\Delta A = 1/N\Sigma_{t_i}|(A^{\mathrm{rMC}}(t_i) - A^{\mathrm{QMC}}(t_i))/A^{\mathrm{QMC}}(t_i)|$ with $N=100$ in two temperature regimes for all structures [sc, bcc, fcc; fm, afm, $J_2=2.5J_1$ (fm), $J_2=5J_1$ (fm)]. The standard deviation of the different structures is shown in brackets.

		$0.1 < T/T_C^{\mathrm{cMC}} < 1$				$1 < T/T_C^{\mathrm{cMC}} < 2$			
	ΔA	$S=1/2$	$S=1$	$S=3/2$	$S=7/2$	$S=1/2$	$S=1$	$S=3/2$	$S=7/2$
C_V	rMC	41.2(7.1)	21.9(4.3)	15.8(2.9)	5.5(2.0)	49.8(25.9)	15.2(9.7)	7.1(5.2)	2.2(3.4)
	cMC	1897.3(951.9)	885.5(413.8)	533.3(171.4)	112.3(12.1)	99.7(34.8)	33.4(11.3)	16.9(5.6)	3.7(1.4)
U	rMC	32.2(11.9)	9.8(5.4)	4.3(3.4)	1.0(1.2)	14.1(9.5)	5.2(4.2)	2.7(2.6)	1.1(1.8)
	cMC	125.5(17.9)	53.9(6.2)	31.5(3.4)	9.(1.0)	25.7(10.4)	10.7(4.2)	5.9(2.3)	1.5(0.6)
S_{m}	rMC	226.2(81.0)	48.9(42.8)	28.2(32.7)	9.3(10.3)	3.7(3.1)	1.3(1.3)	0.8(0.8)	0.7(0.5)
	cMC	3630.(1614.4)	1810.3(646.4)	1087.4(343.0)	223.1(57.0)	6.5(3.3)	2.2(1.4)	1.1(0.8)	0.6(0.5)
F	rMC	12.8(5.0)	3.9(2.2)	1.7(1.4)	0.7(0.7)	1.1(0.8)	0.5(0.3)	0.5(0.3)	0.6(0.4)
	cMC	49.3(6.2)	20.8(2.3)	11.9(1.3)	3.4(0.6)	1.5(0.9)	0.7(0.4)	0.6(0.4)	0.7(0.4)

S. Performing a linear regression over all calculated data sets for different systems yields

$$1/t_S \approx 0.54(1)S + 0.54(2), \tag{10}$$

close to the mean-field value as given by Eq. (8). The mean deviation on the last digit is shown in brackets.

The quality of the analytical expressions for the rescaling functions Eqs. (9) and (10), is demonstrated in Fig. 6(a). Here, we observe for all considered parameters a fair agreement between $\bar{f}(t,S)$ and $f^{\mathrm{approx}}(t,S)$, with the smallest deviations for low temperatures t and high-spin values S.

In order to test the accuracy of this approach, we apply the rescaling scheme to the previously discussed cMC data of model systems. This allows a direct comparison of the temperature dependences obtained by the two-step procedure (fitting+linearizing $1/t_S$) resulting in $f^{\mathrm{approx}}(t,S)$ with the numerically exact QMC results. In contrast to Fig. 6(a), it has been performed for all σ individually and would only be trivial if the rescaling function $f(t,S,\sigma)$ were used. Since in practice, the quantum solution is usually not known *a priori*, we also do not align the classical and quantum solution with respect to the temperature, i.e., we do not enforce $T_C^{\mathrm{rMC}} = T_C^{\mathrm{QMC}}$. To get an impression of the accuracy, we show as an example the heat capacity for the bcc, ferromagnetic nearest-neighbor case (black line in Fig. 1). For all spin quantum numbers, the classical results are found to be significantly improved. A similar accuracy is found for all other considered systems.

Based on the rescaled heat capacity we compute, similar to Eq. (5), the internal energy,

$$U^{\mathrm{rMC}}(T) = U^{\mathrm{cMC}}(T_H) - \int_T^{T_H} C_V^{\mathrm{rMC}}(T)dT. \tag{11}$$

Here we have used that $U^{\mathrm{cMC}}(T_H) \approx U^{\mathrm{QMC}}(T_H)$ and $C_V(T_H) \approx 0$ for sufficiently high cutoff temperatures $T_H > T_C$. The rescaled internal energy Eq. (11) and the rescaled entropy Eq. (5) are compared in Figs. 2 and 3 with the cMC and QMC results. Altogether, the classical description is improved for all considered spin quantum numbers and thermodynamic properties. As expected, deviations are larger for small spin quantum numbers (e.g., $S=1/2$) (see Fig. 1). A major source for the remaining discrepancies are the deviations between the Curie temperatures for small spins and in the classical limit $S \to \infty$.[23] In general, with increasing spin number, the predictive accuracy of rMC improves and already for $S \geq 3/2$, the results are very close to the full QMC calculations. A similar behavior is found for the internal energy and magnetic entropy. For the magnetic free energy (Fig. 4), the deviations between the classical and QM solution are significantly reduced, resulting in a good overall agreement of the rMC and the QMC.

Generally we find that the rescaling approach consistently improves the problematic low-temperature regime. For integrated quantities such as the entropy, internal, and the free energy, the remaining errors accumulate in the low-temperature region due to the backward integration from high to low temperatures by virtue of Eqs. (5) and (11). A consequence is the presence of (unphysical) negative entropies at low temperatures (shaded temperature range at Fig. 4), despite the good description of the rescaled heat capacity both at low and high temperatures with the largest deviations close to the critical temperature.

To quantitatively estimate the accuracy achievable by the rescaling approach, we summarize in Table I the mean deviation in percent (standard deviation of the various structures shown in brackets) between the rMC (first rows) and the cMC (second rows) with the QMC data for different temperature ranges and averaged over all model structures considered in this study. For low temperatures (below the critical temperature), the rMC approach improves the description of the aligned cMC approach considerably and provides already for $S \geq 1$ a good approximate prediction of the quantum-mechanical free energy with an error of less than 4%. For higher temperatures (above the critical temperature), the rMC reduces the deviations between the cMC and the QMC data for all thermodynamic quantities by almost a factor of 2. The fact that the scatter between the different structures, as reflected in the standard deviation shown in Table I, is almost always smaller than the mean deviation and that it consistently decreases with S, demonstrates that the rescaling approach works equally well for all investigated lattice types, magnetic configurations, and number of included interaction

shells. We, therefore, expect a similar accuracy of the proposed rescaling approach for other lattice geometries and if interaction shells beyond second-nearest neighbors are included.

III. APPLICATION OF THE RESCALING MC TO FM bcc IRON

In the following, we employ the rMC approach to compute the magnetic contribution of bcc iron as an example of a realistic magnetic material system. We note that although bcc iron is not an ideal Heisenberg ferromagnet,[12,26,27] the Heisenberg model is an established theoretical approach for describing magnetism in iron providing a surprisingly reasonable description of the system.[7,10–12,15] This material shows a ferromagnetic order with $T_C^{\mathrm{exp}}=1044$ K.[28] However, despite its predominant ferromagnetic coupling, positive (i.e., antiferromagnetic) exchange integrals occur in higher-order shells. These exchange integrals cannot be neglected due to the very long-ranged character of the interactions[15] (magnetic interactions up to the 25 neighbor shell were included) and lead to weak magnetic frustrations which rule out a use of the QMC approach.[29]

To compute the thermodynamic properties, we start with the full Helmholtz free energy $F(T,V)$ for bcc iron including vibronic, electronic, and magnetic contributions in the adiabatic approximation as in Ref. 7,

$$F(T,V) \approx F_{\mathrm{vib}}(T,V) + F_{\mathrm{el}}(T,V) + F_{\mathrm{mag}}(T,V). \qquad (12)$$

Explicit coupling terms such as, e.g., phonon-magnon, phonon-electron, or phonon-phonon interactions are neglected since they are expected to be small.[30,31] The numerical convergence of the calculated $F(T,V)$ is ensured to be below 1 meV/atom for the considered temperature range.[32]

Previous studies indicate that for bcc iron, the first two contributions in Eq. (12) dominate the low-temperature (below room temperature) thermodynamics.[7,33] These contributions are calculated employing the quasiharmonic approximation and finite-temperature DFT (Ref. 34) for F_{vib} and F_{el}, respectively, as discussed in detail in Refs. 7 and 35. The calculations were performed employing the VASP (Ref. 36) package using the projector-augmented wave method[37] within the generalized gradient approximation (Perdew-Burke-Ernzerhof parametrization[38]).

The sum of F_{vib} and F_{el} is shown in Fig. 7 and compared with CALPHAD (Refs. 39 and 40) data. In order to compare our DFT free energies to the CALPHAD free energies F^{CAL}, we align both at a finite temperature (200 K) as in Ref. 35. The strong deviations between the calculated and the experimental free energy and heat capacity (Fig. 8) above room temperature are a consequence of the absence of magnetic contributions. These results clearly highlight the significance of magnetic contributions at these temperatures.[7]

In order to evaluate the magnetic contribution, we start with the comparison of the classical Monte Carlo calculations and the rescaling Monte Carlo scheme for the specific-heat capacity (Fig. 8). Classical Monte Carlo calculations were performed using a $12\times12\times12$ supercell (containing 1728 atoms) including magnetic interactions up to the first

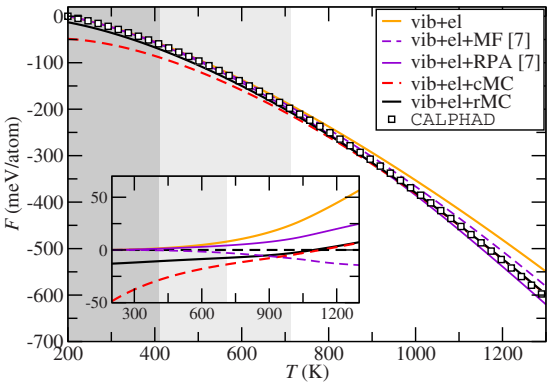

FIG. 7. (Color online) The free energy of bcc iron as a function of temperature. Inset: difference between the different theoretical and the CALPHAD data is shown. For comparison, the theoretical MF and RPA results of Ref. 7 are also shown.

25 neighbor shells. The effective real-space exchange coefficients J entering Eq. (1) have been calculated using the frozen-magnon approach as in Refs. 7 and 16, and performing a Fourier transformation of the obtained reciprocal-space exchange integrals afterward. The magnetic heat capacity is calculated assuming that the magnetic moments of Fe do not significantly change due to the thermal volume expansion and temperature, resulting in $C_V(T) \approx C_P(T)$.[16] Adding the magnetic contribution to $C_P(T)$ (Fig. 8) reproduces a transition from the ferromagnetic to the paramagnetic state. The magnetic transition shows up as peak in the heat capacity (Fig. 8). The resulting critical temperature is $T_C^{\mathrm{cMC}} \approx 1060$ K which is close to the experimental value and similar to previous calculations.[10–12] We note that the rapid change in $C_P(T)$ around the critical temperature causes comparatively large deviations in the experimental measurements in this temperature window.[42] In the paramagnetic regime, the cMC approach reproduces the experimental behavior very well, confirming our finding in the previous section that short-range magnetic order is well captured within the cMC calculations and that quantum effects are not critical in this temperature regime.

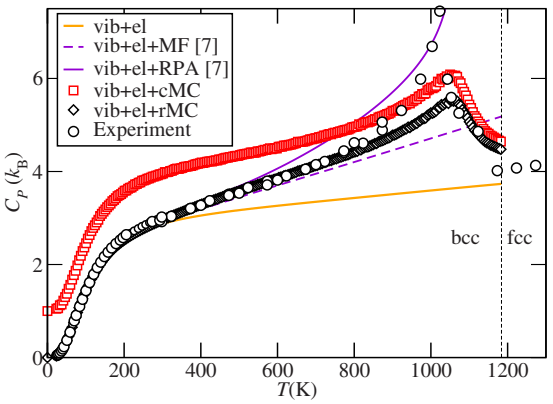

FIG. 8. (Color online) Heat capacity vs temperature for the different theoretical data vs experiment (Ref. 41). The experimental transition temperature (bcc→fcc) $T^{\alpha\gamma}\approx1184$ K is indicated by a dashed line. For comparison, the theoretical MF and RPA results of Ref. 7 are also shown.

To calculate $F_{\mathrm{mag}}^{\mathrm{cMC}}$, we use the calculated cMC internal energy U^{cMC} and the classical entropy S_m^{cMC} aligned to the maximum entropy $S_{\mathrm{m}}^{\mathrm{mag}}(S)$ for the quantum spin system at high temperatures [see Eq. (5)]. Corresponding to the *ab initio* calculated ground-state magnetic moment $2.2\mu_B$, the effective spin quantum number $S=1.1$ is used. In order to align the magnetic free energy at $T=0$ K (the $T=0$ K energy is already included in F_{el}, see Ref. 7) and to obtain the magnetic excitation energies, the $T=0$ K contribution $U_{T=0}^{\mathrm{QM}}(S)$ is subtracted from the calculated $F_{\mathrm{mag}}^{\mathrm{cMC}}$ after the alignment of F and F^{CAL}.[43] The resulting F^{cMC} is shown in Fig. 7. The obtained agreement at high temperatures is excellent. Above the critical temperature, the aligned cMC free energy provides a very good description of the magnetic contribution to the free energy of bcc iron. At lower temperatures, however, the deviations are visible and increase in magnitude with a decrease in the temperature. Below $\approx$700 K, the aligned cMC entropy becomes negative (highlighted by light-gray color), which leads to a wrong asymptotic behavior of the calculated free energy. This region is, therefore, not properly described within the cMC ansatz, although quantitatively the deviations of F^{cMC} from the experimental data remain moderate even at temperatures below 700 K.

We use now the rescaling framework and multiply the cMC data for $C_P(T)$ with the rescaling function given by Eqs. (9) and (10). The results are shown in Fig. 8 (black diamonds) and reveal a significant improvement over the cMC results below the room temperature, yielding an overall excellent agreement of the calculated heat capacity with the available experimental data. The largest deviations occur close to the critical temperature where the finite-size effects in the MC calculations hinder an accurate description of the heat capacity in the thermodynamic limit of infinite system size $L\rightarrow\infty$.[44] Applying our rescaling ansatz to the cMC entropy and internal energy, we derive the rMC free energy (black straight line in Fig. 7). As can be seen, our rescaling approach provides an accurate agreement with the experiment with an error bar of less than 10 meV/atom over the whole temperature range of thermodynamically stable bcc iron. We note, that the temperature below which the rMC entropy becomes negative (indicating the breakdown of this approach) is significantly extended by $\approx$300 K to lower temperatures (marked by the dark shaded region) when compared to the aligned cMC. Our results show that the rescaling procedure is indeed able to correct for the cMC deficiencies in the low-temperature ($T<T_C$) regime and lead to a significant decrease in the errors in the calculated thermodynamic properties.

IV. SUMMARY

In conclusion, based on numerically exact results obtained from spin QMC, we have systematically analyzed deviations between the classical and quantum solution of the Heisenberg model for different model systems. Fundamental differences between both treatments (classical and quantum mechanical) have been discussed for various thermodynamic properties. For high temperatures well above T_C as well as for increasing spin quantum numbers ($S\geq 7/2$) quantities such as the internal energy and the specific-heat capacity approach each other as expected. Aligning the classical magnetic entropy to the corresponding quantum limit allows to predict the free energy from high temperatures down to $\approx T_C$. However, below the critical temperature, the classical treatment deviates significantly compared to the quantum treatment. In order to extend the description to lower temperatures, we propose a rescaling approach which allows to modify the classical heat capacity toward the quantum-mechanical solution. This approach results in a significant improvement of all thermodynamic quantities, and thus allows for an approximate *ad hoc* inclusion of the underlying quantum effects. The obtained rescaling function turned out to be robust with respect to the type of the underlying lattice, the range of interactions (number of included shells), as well as the kind of interaction (ferromagnetic vs antiferromagnetic). The approach has been derived and tested for magnetic systems where magnetic frustration is absent or weak. Further studies are therefore necessary to identify whether it breaks down for strongly frustrated systems. We note also that the accuracy may be further improved by incorporating the dependence of the critical temperature on S.

In Sec. III, the new methodology is applied to ferromagnetic bcc Fe in order to check the applicability of the new scheme to systems where QMC calculations are not feasible. Combined with electronic and vibronic contributions calculated from first principles, a prediction of the thermodynamics of bcc iron is given in the temperature range where it is thermodynamically stable (up to 1200 K). Considering the magnetic contribution, alignment of the calculated classical magnetic entropy to the quantum limit allows an accurate description of the total free energy down to $\approx$700 K. The rescaling framework significantly improves the description of the heat capacity, and allows to extend the prediction range for the free energy down to $\approx$400 K. Importantly, the proposed rescaling approach does not only extend the prediction capability of the cMC method but also provides a possibility to estimate the magnitude of the quantum effects at different temperatures via the magnitude of the discrepancy between the aligned cMC and the rescaled cMC results. Together with analytical approaches covering the low-temperature limit, such as, e.g., spin-wave approximations, the presented approach provides a straightforward tool to describe thermodynamic properties of weakly or unfrustrated magnetic systems over the entire temperature range of thermodynamic stability.

ACKNOWLEDGMENTS

Funding by the collobarative research center SFB 761 "Stahl–*ab initio*" of the Deutsche Forschungsgemeinschaft and the Interdisciplinary Centre for Materials Simulation (ICAMS), which is supported by ThyssenKrupp AG, Bayer MaterialScience AG, Salzgitter Mannesmann Forschung GmbH, Robert Bosch GmbH, Benteler Stahl/Rohr GmbH, Bayer Technology Services GmbH, and the state of North-Rhine Westphalia as well as the European Commission in the framework of the European Regional Development Fund (ERDF), is gratefully acknowledged.

APPENDIX: MEAN-FIELD SOLUTION OF $f(t,S)$ FOR LOW TEMPERATURES

Within mean-field approximation, the internal energy is proportional to the squared magnetization,

$$U^{\mathrm{MF}}(t,S) \sim m^{\mathrm{MF}}(t,S)^2, \tag{A.1}$$

where the latter is given by

$$m^{\mathrm{MF}}(t,S) \sim B_S\left(\frac{3S}{S+1}\frac{m(t,S)}{t}\right) \tag{A.2}$$

including the Brillouin function,

$$B_S(x) = \frac{2S+1}{2S}\coth\left(\frac{2S+1}{2S}x\right) - \frac{1}{2S}\coth\left(\frac{1}{2S}x\right). \tag{A.3}$$

For $S\to\infty$, this function transforms into the Langevin function,

$$B_{S\to\infty}(x) = L(x) = \coth(x) - \frac{1}{x}. \tag{A.4}$$

For low temperature, i.e., $x \gg 1$, one obtains

$$B_S(x \gg 1) = 1 - \frac{\exp(-x/S)}{S}, \tag{A.5}$$

$$L(x \gg 1) = 1 - 1/x. \tag{A.6}$$

Combining Eqs. (A.1)–(A.6), one obtains straightforwardly the low-temperature expansion for the heat capacity,

$$C^{\mathrm{MF}}(t,S) = -\frac{3}{2}k_B\frac{S}{S+1}\frac{dm^2(t,S)}{dt} \tag{A.7}$$

as

$$C^{\mathrm{MF}}(t\to 0,S) \approx k_B\left(\frac{2t_S^{\mathrm{MF}}/t}{\exp(t_S^{\mathrm{MF}}/t)}\right)^2, \tag{A.8}$$

$$C^{\mathrm{MF}}(t\to 0,S\to\infty) \approx \frac{k_B}{2}\left(1 + \frac{1}{\sqrt{1-4/3t}}\right) \tag{A.9}$$

with the spin-dependent variable,

$$1/t_S^{\mathrm{MF}} \equiv 2/3(S+1). \tag{A.10}$$

Therewith one readily can compute the ratio of the quantum and classical ($S\to\infty$) heat capacity within MF,

$$\lim_{t\to 0} f^{\mathrm{MF}}(t,S) = \lim_{t\to 0} C^{\mathrm{MF}}(t,S)/C^{\mathrm{MF}}(t,S\to\infty) \tag{A.11}$$

in the low-temperature limit $t\to 0$ and we obtain

$$f^{\mathrm{MF}}(t\to 0,S) = \left(\frac{2t_S^{\mathrm{MF}}/t}{\exp(t_S^{\mathrm{MF}}/t)}\right)^2. \tag{A.12}$$

*koermann@mpie.de

[1] P. Souvatzis and O. Eriksson, Phys. Rev. B **77**, 024110 (2008).
[2] A. Debernardi, M. Alouani, and H. Dreyssé, Phys. Rev. B **63**, 064305 (2001).
[3] A. Siegel, K. Parlinski, and U. D. Wdowik, Phys. Rev. B **74**, 104116 (2006).
[4] L. Kaufman, E. V. Clougherty, and R. J. Weiss, Acta Metall. **11**, 323 (1963).
[5] B. Hallstedt, D. Djurovic, J. von Appen, R. Dronskowski, A. Dick, F. Körmann, T. Hickel, and J. Neugebauer, CALPHAD **34**, 129 (2010).
[6] H. Hasegawa and D. G. Pettifor, Phys. Rev. Lett. **50**, 130 (1983).
[7] F. Körmann, A. Dick, B. Grabowski, B. Hallstedt, T. Hickel, and J. Neugebauer, Phys. Rev. B **78**, 033102 (2008).
[8] L. Sandoval, H. M. Urbassek, and P. Entel, Phys. Rev. B **80**, 214108 (2009).
[9] T. Hickel, A. Dick, B. Grabowski, F. Körmann, and J. Neugebauer, Steel Res. Int. **80**, 4 (2009).
[10] N. M. Rosengaard and B. Johansson, Phys. Rev. B **55**, 14975 (1997).
[11] M. Ležaić, P. Mavropoulos, and S. Blügel, Appl. Phys. Lett. **90**, 082504 (2007).
[12] A. V. Ruban, S. Khmelevskyi, P. Mohn, and B. Johansson, Phys. Rev. B **75**, 054402 (2007).
[13] J. Rusz, L. Bergqvist, J. Kudrnovský, and I. Turek, Phys. Rev. B **73**, 214412 (2006).
[14] G. Y. Gao, K. L. Yao, E. Şaşioğlu, L. M. Sandratskii, Z. L. Liu, and J. L. Jiang, Phys. Rev. B **75**, 174442 (2007).
[15] M. Pajda, J. Kudrnovsky, I. Turek, V. Drchal, and P. Bruno, Phys. Rev. B **64**, 174402 (2001).
[16] F. Körmann, A. Dick, T. Hickel, and J. Neugebauer, Phys. Rev. B **79**, 184406 (2009).
[17] A. W. Sandvik and J. Kurkijärvi, Phys. Rev. B **43**, 5950 (1991).
[18] H. G. Evertz, Adv. Phys. **52**, 1 (2003).
[19] P. Henelius and A. W. Sandvik, Phys. Rev. B **62**, 1102 (2000).
[20] E. Y. Loh, J. E. Gubernatis, R. T. Scalettar, S. R. White, D. J. Scalapino, and R. L. Sugar, Phys. Rev. B **41**, 9301 (1990).
[21] A. Albuquerque *et al.*, J. Magn. Magn. Mater. **310**, 1187 (2007).
[22] M. E. J. Newman and G. T. Barkema, *Monte Carlo Methods in Statistical Physics* (Oxford University Press, USA, 1999).
[23] The critical temperature within the quantum case does not strictly follow $T_C(S) \sim JS(S+1) = \tilde{J}$ as was, e.g., recently shown using high-temperature series expansion [J. Phys.: Condens. Matter **16**, 8653 (2004)]. The complex dependence of $T_C(S)$ is, however, beyond the scope of the present paper.
[24] The exclusions are $T_C(S)$ as discussed in the text and the integration constant $U^{\mathrm{QMC}}(0)$ for the internal energy, which cannot be determined solely from the heat capacity. To determine $U^{\mathrm{QMC}}(0)$, we use $U^{\mathrm{cMC}}(T_h) \equiv U^{\mathrm{QMC}}(T_h)$, which holds true for high temperatures T_h. For all considered systems, the choice $T_h = 3T_C$ was in this respect sufficient.
[25] The nearest-neighbor antiferromagnetic fcc lattice is known to be frustrated, see, e.g. [J. Low Temp. Phys. **146**, 581 (2007)], and is therefore not considered in this study.
[26] V. Heine, A. I. Liechtenstein, and O. N. Mryasov, Europhys.

Lett. **12**, 545 (1990).
[27] A. V. Ruban, S. Shallcross, S. I. Simak, and H. L. Skriver, Phys. Rev. B **70**, 125115 (2004).
[28] J. Crangle and G. M. Goodman, Proc. R. Soc. London, Ser. A **321**, 477 (1971).
[29] By taking ten shells into account the average sign $\langle\sigma\rangle_T$ decreases to 10^{-3} for temperatures below $2T_C$. To achieve statistical errors of less than 5%, the calculation time on a conventional computer is on the order of years for a single temperature calculation.
[30] R. F. Sabiryanov and S. S. Jaswal, Phys. Rev. Lett. **83**, 2062 (1999).
[31] B. Grabowski, L. Ismer, T. Hickel, and J. Neugebauer, Phys. Rev. B **79**, 134106 (2009).
[32] The following parameters have been used. Vibrational part: 54-atom supercell; ≈27 000 **k**-points·atom (kp·a); plane-wave cutoff energy E_{cut}=340 eV. Electronic part: ≈40 000 kp·a; E_{cut}=340 eV. Magnetic part: ≈7000 kp·a; E_{cut}=400 eV; ≈3000 **q** points for the Fourier transformation $J_{ij}=\Sigma_{\mathbf{q}}J_{\mathbf{q}}\exp[i\mathbf{q}\mathbf{R}_{ij}]$.
[33] X. Sha and R. E. Cohen, Phys. Rev. B **73**, 104303 (2006).
[34] N. D. Mermin, Phys. Rev. **137**, A1441 (1965).
[35] B. Grabowski, T. Hickel, and J. Neugebauer, Phys. Rev. B **76**, 024309 (2007).
[36] G. Kresse and J. Furthmüller, Phys. Rev. B **54**, 11169 (1996).
[37] P. E. Blöchl, Phys. Rev. B **50**, 17953 (1994).
[38] J. P. Perdew, K. Burke, and M. Ernzerhof, Phys. Rev. Lett. **77**, 3865 (1996).
[39] L. Kaufman and H. Bernstein, *Computer Calculation of Phase Diagrams* (Academic, New York, 1970).
[40] N. Saunders and A. P. Miodownik, *Calphad (Calculation of Phase Diagrams): A Comprehensive Guide* (Pergamon, Oxford, 1998).
[41] Y. S. Touloukian, R. K. Kirby, R. E. Taylor, and P. D. Desai, *Thermophysical Properties of Matter* (IFI/Plenum, New York, 1975), Vol. 12; D. C. Wallace, P. H. Sidles, and G. C. Danielson, J. Appl. Phys. **31**, 168 (1960).
[42] P. D. Desai, J. Phys. Chem. Ref. Data **15**, 967 (1986).
[43] Strictly speaking, the internal energy at 200 K has to be subtracted at which the calculated results are aligned to the CALPHAD data. Due to the negligible contribution of $C_P(T<200\ \text{K})\approx 0=dU/dT$, $U^{\text{QM}}_{T=0\ \text{K}}\approx U^{\text{QM}}_{T=200\ \text{K}}$ is assumed.
[44] If the heat capacity shows a finite cusp with a magnitude $C_P(T_C)=C_P^{\max}$, a finite-size ansatz can be used to extrapolate the dependence $C_P^{\max}(L)$ on system size L. Depending on the finite-size scaling fit, the system size required to obtain, e.g., 50% of $C_P^{\max}$ may result in system sizes containing up to 10^7 atoms [see, e.g., Phys. Rev. B **43**, 6087 (1991)] which renders the problem to be computationally unfeasible.